Utrecht University

Debye Institute for Nanomaterials Science

Quantum Nanophotonics Group

Simulations of femtosecond laser excitation in bulk silica

Author:
Charly Beulenkamp BSc

Supervisors:
Dr. J. Hernández-Rueda
Dr. D. van Oosten

July 5, 2017

Abstract

A model to simulate the interaction between ultrashort light pulses and bulk fused silica is presented. Starting from Maxwell's equations, an equation for computing light propagation is derived using the slowly varying envelope approximation. Two third order nonlinear effects, the Kerr effect and Raman scattering, are taken into account. The model also takes into account the generation of an electron plasma by strong field ionization and impact ionization. To describe this process Rethfeld's multiple rate equation is used. The transmission profiles predicted by the simulations are compared with experimental transmission images of electron plasma in silica.

Contents

1 Introduction

Since the invention of the laser in the sixties their usefulness in science, industry and health have stimulated research into their properties. Developments in laser technology have increased control over wavelength, pulse energy, pulse shape and more. In particular the development of mode-locking and chirped pulse amplification techniques have given access to femtosecond laser pulses with pulse energies far above 1 mJ and pulse durations below 10 fs.

A technologically relevant and interesting application of such ultrashort laser pulses is the micromachining of dielectric materials [15] [7]. This involves focusing the pulse in the bulk of the dielectric. In the focus, electrons are excited to the conduction band by the strong electric field via strong field ionization (i.e. multiphoton and tunneling ionization). These electrons are then heated by single photon absorption and excite even more electrons via scattering. The density and temperature distributions of the electron plasma determine the modification of the material. To use femtosecond laser pulses as a tool it is therefore important to understand and be able to predict how the plasma forms.

So far, our group has used the finite-difference time-domain method (FDTD) for simulations of ablation of the surfaces of silica [4] and silicon-on-insulator [22]. The disadvantage of this method is that it requires high resolution, enough to resolve the wavelength of the light. This becomes particularly troublesome when one wants to take into account the heating of the plasma, which requires a matrix differential equation (known as the multiple rate equation (MRE)) to be solved for every point. There is a widely used model [16] [6] [5] for the propagation of femtosecond laser pulses which makes use of the slowly varying envelope approximation to reduce the problem to that of solving the non-linear Schrödinger equation. The slowly varying nature of the envelope means that a much lower resolution can be used. This report presents such a model supplemented with the aforementioned MRE model for plasma heating and methods to enhance numerical efficiency.

First an equation will be derived which allows the computation of the evolution of the electric field in absence of nonlinear effects. Nonlinear polarization effects will be added to it, and a model will be presented for the generation and evolution of the plasma and its effect on the propagation of the electric field. Some numerical methods will then be presented which are used to implement the model into code. Transient transmission images obtained using a pump-probe arrangement [20] are then compared with the transmission predicted by simulations.

2 Theory

2.1 The Schrödinger Equation for the envelope

2.1.1 Maxwell's Equations

The natural starting point for describing the propagation of electromagnetic fields is Maxwell's equations

$$\begin{aligned}
\nabla \cdot \mathbf{E} &= \frac{1}{\epsilon_0}(\rho - \nabla \cdot \mathbf{P}), \\
\nabla \cdot \mathbf{B} &= 0, \\
\nabla \times \mathbf{E} &= -\frac{\partial \mathbf{B}}{\partial t}, \\
\nabla \times \mathbf{B} &= \mu_0(\mathbf{J} + \frac{\partial}{\partial t}(\epsilon_0 \mathbf{E} + \mathbf{P}) + \nabla \times \mathbf{M}).
\end{aligned} \tag{2.1}$$

Combining the third and fourth equations gives us

$$\nabla \times (\nabla \times \mathbf{E}) = -\nabla^2 \mathbf{E} + \nabla(\nabla \cdot \mathbf{E}) = -\mu_0 \frac{\partial \mathbf{J}}{\partial t} - \frac{1}{c^2}\frac{\partial^2}{\partial t^2}\mathbf{E} - \mu_0\left(\frac{\partial^2 \mathbf{P}}{\partial t^2} + \frac{\partial}{\partial t}\nabla \times \mathbf{M}\right). \tag{2.2}$$

We will start by studying unexcited fused silica, so $\rho = 0$. The magnetization $\mathbf{M}$ can be neglected because the magnetic susceptibility at optical frequencies is generally extremely small. Longitudinal waves will be neglected by setting $\nabla \cdot \mathbf{E}$. This yields the wave equation

$$\nabla^2 \mathbf{E} - \frac{1}{c^2}\frac{\partial^2}{\partial t^2}\mathbf{E} = \mu_0\left(\frac{\partial \mathbf{J}}{\partial t} + \frac{\partial^2 \mathbf{P}}{\partial t^2}\right), \tag{2.3}$$

where $c = (\mu_0 \epsilon_0)^{-1/2}$ is the speed of light in vacuum.

2.1.2 The Linear Part

First consider the wave equation with only the first order susceptibility

$$\mathbf{P}^{(1)}(\mathbf{x}, t) = \epsilon_0 \int_{-\infty}^{t} \chi^{(1)}(\mathbf{x}, t - t')\mathbf{E}(\mathbf{x}, t')dt', \tag{2.4}$$

resulting in the wave equation

$$\nabla^2 \mathbf{E} - \frac{1}{c^2}\frac{\partial^2}{\partial t^2}\left(\mathbf{E} + \int_{-\infty}^{t} \chi^{(1)}(\mathbf{x}, t - t')\mathbf{E}(\mathbf{r}, t')dt'\right) = 0. \tag{2.5}$$

In the frequency domain ($\tilde{\mathbf{E}} = \tilde{\mathbf{E}}(\mathbf{x}, \omega)$) this simplifies to

$$\nabla^2 \tilde{\mathbf{E}} + \frac{\omega^2}{c^2}\left(1 + \chi^{(1)}(\omega)\right)\tilde{\mathbf{E}} = \nabla^2 \tilde{\mathbf{E}} + \frac{\omega^2 n^2(\omega)}{c^2}\tilde{\mathbf{E}} = 0, \tag{2.6}$$

where refractive index $n(\omega)$ can be computed using the Sellmeier equation [11]. So now we have

$$[\nabla^2 + k(\omega)^2]\tilde{\mathbf{E}} = 0, \tag{2.7}$$

where $k(\omega) = \frac{n(\omega)\omega}{c}$. For the purposes of computation it is more convenient to have an equation which contains only first order derivatives to some variable. To find such an

equation we can decompose the electric field of a light pulse moving in the z-direction into a carrier wave and an envelope $\mathbf{A}$,

$$\mathbf{E}(\mathbf{x},t) = \frac{1}{2}\left[\mathbf{A}(\mathbf{x},t)e^{i(k_0 z-\omega_0 t)} + c.c.\right], \tag{2.8}$$

where we choose ω_0 to be the frequency around which $\tilde{\mathbf{E}}(\mathbf{x},\omega)$ has a peak and $k_0 = k(\omega_0)$. In the frequency domain we thus have

$$\tilde{\mathbf{E}}(\mathbf{x},\omega) = \frac{1}{2}\left[\tilde{\mathbf{A}}(\mathbf{x},\omega-\omega_0)e^{ik_0 z} + \bar{\tilde{\mathbf{A}}}(\mathbf{x},\omega+\omega_0)e^{-ik_0 z}\right] = 0. \tag{2.9}$$

We can now rewrite the wave equation into a useful equation for the envelope by making the slowly varying envelope approximation. If we assume that $\mathbf{A}$ varies slowly in time with respect to the carrier wave, it will be peaked around zero in the frequency domain. So for $\omega \approx \omega_0$ we have

$$\tilde{\mathbf{E}}(\mathbf{x},\omega) \approx \frac{1}{2}\tilde{\mathbf{A}}(\mathbf{x},\omega-\omega_0)e^{ik_0 z}, \tag{2.10}$$

which allows us to separate the wave equation into the positive and negative frequency parts. We then get

$$[\nabla^2 + k(\omega)^2]\tilde{\mathbf{E}} = \frac{1}{2}[\nabla_\perp^2\tilde{\mathbf{A}} + \frac{\partial^2\tilde{\mathbf{A}}}{\partial z^2} + 2ik_0\frac{\partial\tilde{\mathbf{A}}}{\partial z} + (k^2(\omega)-k_0^2)\tilde{\mathbf{A}}]e^{ik_0 z} = 0, \tag{2.11}$$

where $\tilde{\mathbf{A}} = \tilde{\mathbf{A}}(\mathbf{x},\omega-\omega_0)$ If we assume that the envelope is also slowly varying in the z direction, we can neglect the second derivative to z and shift the frequencies to get

$$\frac{1}{2}[\nabla_\perp^2 + 2ik_0\frac{\partial}{\partial z} + k^2(\omega_0+\omega) - k_0^2]\tilde{\mathbf{A}}(\mathbf{x},\omega) = 0. \tag{2.12}$$

As we are only interested in some timeframe centered around the arrival of the pulse, it is convenient to switch to temporal co-moving coordinates $\tau = t - \frac{z}{v_g}$ and $\eta = z$, where v_g is the group velocity, i.e. the speed at which the envelope travels when only the first order susceptibility is taken into account. Under this coordinate transformation, the derivatives transform as

$$\begin{array}{lll} \text{Time domain} & & \text{Frequency domain} \\ \frac{\partial}{\partial t} = \frac{\partial\tau}{\partial t}\frac{\partial}{\partial\tau} + \frac{\partial\eta}{\partial t}\frac{\partial}{\partial\eta} = \frac{\partial}{\partial\tau} & \longrightarrow & -i\omega_t = -i\omega_\tau \\ \frac{\partial}{\partial z} = \frac{\partial\tau}{\partial z}\frac{\partial}{\partial\tau} + \frac{\partial\eta}{\partial z}\frac{\partial}{\partial\eta} = -\frac{1}{v_g}\frac{\partial}{\partial\tau} + \frac{\partial}{\partial\eta} & \longrightarrow & \frac{\partial}{\partial z} = \frac{i\omega_\tau}{v_g}\frac{\partial}{\partial\tau} + \frac{\partial}{\partial\eta}. \end{array} \tag{2.13}$$

The envelope equation then becomes (now using $\omega = \omega_\tau$)

$$\frac{1}{2}[\nabla_\perp^2 + 2ik_0\frac{\partial}{\partial\eta} - \frac{2k_0\omega}{v_g} + k^2(\omega_0+\omega) - k_0^2)]\tilde{\mathbf{A}} = 0. \tag{2.14}$$

As $\tilde{\mathbf{A}}$ is sharply peaked around $\omega = 0$ we can further approximate

$$\begin{aligned} k_0^2 - k^2(\omega+\omega_0) =& (k_0 + k(\omega+\omega_0))(k_0 - k(\omega+\omega_0)) \approx 2k_0(k_0 - k(\omega+\omega_0)) \\ \approx& -2k_0\left(\frac{\omega}{v_g} + \frac{\beta\omega^2}{2}\right), \end{aligned}$$

where β is the group velocity dispersion. Finally, we can cast the envelope equation in the form of the Schrödinger equation

$$i\frac{\partial\tilde{\mathbf{A}}}{\partial\eta} = \left[-\frac{\nabla_\perp^2}{2k_0} + \frac{\beta(-i\omega)^2}{2}\right]\tilde{\mathbf{A}}. \tag{2.15}$$

In the time domain this becomes

$$i\frac{\partial \mathbf{A}}{\partial \eta} = \left[-\frac{\nabla_\perp^2}{2k_0} + \frac{\beta}{2}\frac{\partial^2}{\partial \tau^2} \right] \mathbf{A}. \tag{2.16}$$

Note that we only moved some terms in the wave equations to the right-hand side and divided the whole by k_0, so contributions from currents and polarization on the right-hand side of the wave equation (2.3) can be added by extracting from them the terms of the form $F\mathbf{A}e^{i(k_0 z - \omega_0 t)}$ and then adding $\frac{F}{k_0}\mathbf{A}$ to the right-hand side of the envelope equation.

We can estimate the significance of the GVD by considering the equation $\frac{\partial^2 \mathbf{A}}{\partial \tau^2} - \frac{2i}{\beta}\frac{\partial \mathbf{A}}{\partial \eta} = 0$ with an initial $\mathbf{A}$ which is Gaussian in time with $\mathbf{A}(\tau) \propto \exp(-\tau^2/t_p^2)$. The solution is a Gaussian beam with Rayleigh length $\eta_R = t_p^2/2\beta$. For a femtosecond pulse with $t_p = 100$ fs traveling through silica with $\beta = 36$ fs^2/mm [12], one thus finds that temporal broadening occurs on the scale of $\eta_R = 13.9$ cm. The simulations described in this text consider only the area where plasma forms, which is shorter than 1 mm, so the GVD can be neglected.

2.2 Nonlinear Polarization

There are two significant nonlinear polarization effects, both of them third order as inversion symmetry of fused silica rules out second order nonlinear polarization. The first is the Kerr effect, which is instantaneous

$$\mathbf{P}^{(3)}_{\text{Kerr}}(\mathbf{x}, t) = \epsilon_0 \chi^{(3)}_{\text{Kerr}} |\mathbf{E}|^2 \mathbf{E}. \tag{2.17}$$

The second is a delayed effect known as Raman scattering, which is due to molecular vibrations induced by light. It can be modelled as [5]

$$\mathbf{P}^{(3)}_{\text{Raman}}(\mathbf{x}, t) = \epsilon_0 \mathcal{Q}_R(\mathbf{x}, t)\mathbf{E}(\mathbf{x}, t), \tag{2.18}$$

where $\mathcal{Q}_R$ is the solution to the damped harmonic oscillator problem corresponding to the molecular vibrations

$$\frac{\partial^2 \mathcal{Q}_R}{\partial t^2} + 2\Gamma\frac{\partial \mathcal{Q}_R}{\partial t} + (\omega_R^2 + \Gamma^2)\mathcal{Q}_R = \frac{\omega_R}{\Omega_0}\frac{\mu^2}{\hbar^2}|\mathbf{E}|^2, \tag{2.19}$$

with $\omega_R^{-1} = 12$ fs and $\Gamma^{-1} = 50$ fs [23]. One can show that the Green's function for this problem is

$$G(t, t') = \Theta(t - t')\frac{e^{-\Gamma(t-t')}}{\omega_R}\sin(\omega_R(t - t')), \tag{2.20}$$

where Θ is the Heaviside step function. The solution is thus

$$\begin{aligned} \mathcal{Q}_R(t) &= \frac{\omega_R}{\Omega_0}\frac{\mu^2}{\hbar^2}\int_{-\infty}^{\infty} dt' G(t, t')|\mathbf{E}(t')|^2 \\ &= \frac{\mu^2}{\hbar^2\Omega_0}\int_{-\infty}^{t} dt' e^{-\Gamma(t-t')}\sin(\omega_R(t - t'))|\mathbf{E}(t')|^2 \\ &= \frac{\mu^2}{\hbar^2\Omega_0}\int_{0}^{\infty} dt' e^{-\Gamma t'}\sin(\omega_R t')|\mathbf{E}(t - t')|^2 \\ &= \frac{\mu^2}{\hbar^2\Omega_0}\frac{\omega_R}{\omega_R^2 + \Gamma^2}\int_{0}^{\infty} dt' \mathcal{R}(t')|\mathbf{E}(t - t')|^2, \end{aligned} \tag{2.21}$$

where $\mathcal{R}(t) = \frac{\omega_R^2 + \Gamma^2}{\omega_R} e^{-\Gamma t'}\sin(\omega_R t')$, which satisfies $\int_0^\infty dt \mathcal{R}(t) = 1$. This choice ensures that the order of magnitude of the convolution of $\mathcal{R}$ and $|\mathbf{E}|^2$ is the same as that of $|\mathbf{E}|^2$. This notation allows one to more easily relate the Kerr effect and Raman scattering.

2.2.1 Effect on the electric field

The total third order nonlinear polarization is thus

$$\mathbf{P}^{(3)}(t) = \epsilon_0 \left[\chi^{(3)}_{\text{Kerr}} |\mathbf{E}(t)|^2 + \frac{\mu^2}{\hbar^2 \Omega_0} \frac{\omega_R}{\omega_R^2 + \Gamma^2} \int_0^\infty dt' \mathcal{R}(t') |\mathbf{E}(t-t')|^2 \right] \mathbf{E}(t). \tag{2.22}$$

To find the effect on the electric field we need to extract the part centered at frequency $+\omega_0$ and take two time derivatives (third harmonic generation will be neglected because of the lack of phase matching). We start by considering

$$\begin{aligned} &|\mathbf{E}|^2 \mathbf{E} = \\ &= \frac{1}{8} \left[\mathbf{A}^2 e^{-2i\omega_0} + 2|\mathbf{A}|^2 + \bar{\mathbf{A}}^2 e^{2i\omega_0 t} \right] \times \left[\mathbf{A}(t) e^{-i\omega_0 t} + \bar{\mathbf{A}} e^{i\omega_0 t} \right] \\ &= \frac{1}{8} \left[2\mathbf{A}^2 \bar{\mathbf{A}} e^{-i\omega_0 t} + 2|\mathbf{A}|^2 \mathbf{A} e^{-i\omega_0 t} + ... \right] \\ &= \frac{3}{8} \left[|\mathbf{A}|^2 \mathbf{A} e^{-i\omega_0 t} + ... \right], \end{aligned} \tag{2.23}$$

and thus

$$\begin{aligned} &\frac{\mu_0}{k_0} \frac{\partial^2}{\partial t^2} \left(\epsilon_0 \chi^{(3)}_{\text{Kerr}} |\mathbf{E}|^2 \mathbf{E} \right) = \\ &= -\frac{3\omega_0^2}{8 k_0 c^2} \chi^{(3)}_{\text{Kerr}} \left[|\mathbf{A}|^2 \mathbf{A} e^{-i\omega_0 t} + ... \right]. \end{aligned} \tag{2.24}$$

In absence of Raman scattering we have $\chi^{(3)}_{\text{Kerr}} = \frac{4 n_2 n_0^2 \epsilon_0 c}{3}$, where n_2 is the nonlinear refractive index defined as $n = n_0 + n_2 I$. This nonlinear refractive index is measured using the z-scan technique [6]. For these measurements the envelope of the probing light is approximately constant on the timescale of Raman scattering. This means that $\int_0^\infty dt' \mathcal{R}(t') |\mathbf{E}(t-t')|^2 \approx |\mathbf{E}(t')|^2$ and so the Raman scattering term takes the form of the Kerr effect term and contributes directly to the nonlinear refractive index. This contribution can be characterized by $f_R = 0.18$, the fraction of the nonlinear refractive index which is due to Raman scattering. Using this fact and the expression in 2.24, we can write the effect of nonlinear polarization on the envelope as

$$\begin{aligned} i \left(\frac{\partial \mathbf{A}}{\partial \eta} \right)_{\text{Nonlin}} &= \frac{\mu_0}{k_0} \frac{\partial^2 \mathbf{P}^{(3),+\omega_0}}{\partial t^2} \\ &= -k_0 n_2 \frac{\epsilon_0 c}{2} \left[(1 - f_R) |\mathbf{A}|^2 + f_R \int_0^\infty dt' \mathcal{R}(t') |\mathbf{A}(t-t')|^2 \right] \mathbf{A}, \end{aligned} \tag{2.25}$$

where $n_2 = 3.54 \times 10^{-20} m^2/W^2$ [16].

2.3 The Electron Plasma

2.3.1 Strong-Field Ionization

The fused silica used in ablation experiments has a band gap of $\Delta = 9$ eV, while a photon with a vacuum wavelength of 800 nm has an energy of only $\hbar\omega_0 = 1.56$ eV. The light can thus only excite electrons to the conduction band via multi-photon absorption and electron tunneling in the strong field limit. Keldysh [10] derived an expression for the transition rate between the conduction and valence band which is given by

$$W_{\mathrm{SFI}} = \frac{2\omega_0}{9\pi}\left(\frac{\mu\omega_0}{\hbar\sqrt{\gamma_1}}\right)^{3/2} \mathcal{Q}(\gamma, x) \times \exp\left(- \pi\lfloor x+1\rfloor \frac{\mathcal{K}(\gamma_1) - \mathcal{E}(\gamma_1)}{\mathcal{E}(\gamma_2)}\right), \tag{2.26}$$

where $\gamma = \frac{\omega_0\sqrt{\mu\Delta}}{e|\mathbf{E}|}$, $x = \frac{2}{\pi}\frac{\Delta}{\hbar\omega}\frac{\mathcal{E}(\gamma_2)}{\sqrt{\gamma_1}}$, $\gamma_1 = \gamma^2/(1+\gamma^2)$, $\gamma_2 = 1/(1+\gamma^2)$, μ is the reduced mass of the electron and the hole, the functions $\mathcal{K}$ and $\mathcal{E}$ are complete elliptic integrals of the first and second kind, and

$$\mathcal{Q}(\gamma, x) = \sqrt{\frac{\pi}{2\mathcal{K}(\gamma_2)}} \times \sum_{n=0}^{\infty} \exp\left(- n\pi \frac{\mathcal{K}(\gamma_1) - \mathcal{E}(\gamma_1)}{\mathcal{E}(\gamma_2)}\right) \Phi\left(\frac{\pi^2(\lfloor x+1\rfloor) - x + n}{2\mathcal{K}(\gamma_2)\mathcal{E}(\gamma_2)}\right). \tag{2.27}$$

Due to the absorption of light the amplitude of the envelope decreases. The energy density averaged over one period is $\mathcal{E} = \frac{n^2\epsilon_0}{2}|\mathbf{A}|^2$. The decrease in energy density due to strong field ionization over a time $\Delta\tau$ is $\Delta\mathcal{E} = -\tilde{\Delta} W_{\mathrm{SFI}}\Delta\tau$, where $\tilde{\Delta} = (\Delta + U_p)$ is the effective ionization potential consisting of the bandgap Δ and the ponderomotive energy $U_p = \frac{e^2|\mathbf{A}|^2}{4\omega_0^2}$ that the ionized electron will have in the electric field. The new amplitude is thus

$$|\mathbf{A}'| = \sqrt{|\mathbf{A}|^2 - 2\Delta\tau\frac{W_{\mathrm{SFI}}\tilde{\Delta}}{n^2\epsilon_0}} = |\mathbf{A}|\sqrt{1 - 2\Delta\tau\frac{W_{\mathrm{SFI}}\tilde{\Delta}}{n^2\epsilon_0|\mathbf{A}|^2}}. \tag{2.28}$$

2.3.2 Plasma evolution: the multiple rate equation

Electrons that have been excited to the conduction band can absorb photons from the laser field, increasing their kinetic energy. When their energy is high enough, they can ionize a valence band electron by means if a collision. This process is known as impact ionization. The newly ionized electrons will also be heated and can in turn produce more ionized electrons through impact ionization. The resultant rapid growth of the plasma is therefore known as avalanche ionization. A full treatment of the collisional integrals was done by Kaiser et al [9]. Because it is computationally cumbersome even when considering a single point with constant electric strength, Rethfeld [13] proposed a simplified model known as the multiple rate equation which reproduces the important physical results. This model will be used here to compute the generation of the electron plasma.

The local electron density ρ is divided into bins ρ_i according to their energy above the band gap in units of the photon energy, i.e. ρ_i is the local density of electrons with energy $i\hbar\omega_0$. Strong field ionization adds electrons to the bottom of the conduction band ρ_0. Single photon absorption transfers electrons to higher bins at a rate $W_{1\mathrm{p}}$. Electrons can ionize valence band electrons at a rate α when their energy exceeds the critical energy $E_{\mathrm{imp}} = (1 + \frac{\mu}{m_v})(\Delta + U_p)$. The factor $(\Delta + U_p)$ is the effective ionization potential consisting of the bandgap and the ponderomotive energy $U_p = \frac{e^2|\mathbf{A}|^2}{4mu\omega_0^2}$ that the freely moving conduction band electrons have in the laser field. Here μ is the reduced mass of the conduction band

electrons and the valence band holes, which have effective masses m_c and m_v respectively. The factor of $(1 + \frac{\mu}{m_v})$ is due to momentum conservation. The relevant parameters here are the strong field ionization rate W_{SFI} and the single photon absorption rate $W_{1\mathrm{p}}$. The impact ionization rate is set at $\alpha = 6.0 \times 10^{15}\mathrm{s}^{-1}$, since its precise value does not matter as long as $\alpha \gg W_{1\mathrm{p}}$ [13]. The full set of equations is thus

$$\begin{aligned}
\dot{\rho_0} &= -W_{1\mathrm{p}}\rho_0 + W_{\mathrm{SFI}} + 2\alpha \sum_{i=j}^{k} \rho_i \,, \\
\dot{\rho_1} &= -W_{1\mathrm{p}}\rho_1 + W_{1\mathrm{p}}\rho_0 \,, \\
&\vdots \\
\dot{\rho_j} &= -(W_{1\mathrm{p}} + \alpha)\rho_j + W_{1\mathrm{p}}\rho_{j-1} \,, \\
&\vdots \\
\dot{\rho_k} &= -\alpha\rho_k + W_{1\mathrm{p}}\rho_{k-1} \,,
\end{aligned} \tag{2.29}$$

where $j = \lceil E_{\mathrm{imp}}/(\hbar\omega_0) \rceil$. The single photon absorption will be taken to be independent of the electron energy, and derived in the next section by considering the total photon absorption due to the plasma. Photons are absorbed when electrons collide with the lattice or other electrons, thus we will need to know the rate at which these collisions happen. Although the system is not in equilibrium, a temperature can be assigned to the gas based on the average energy per electron [3]

$$\frac{3}{2}k_B T = \frac{\sum_{j=0}^{k} j\hbar\omega_0\rho_j}{\sum_{j=0}^{k}\rho_j}. \tag{2.30}$$

By modeling the electron plasma as a classical gas one can derive an electron-electron scattering rate

$$\Gamma_{\text{e-e}} = \frac{4\pi\epsilon_0}{e^2}\sqrt{\frac{6}{m_c}}(k_B T)^{3/2}. \tag{2.31}$$

Combining the electron-electron and electron-lattice scattering rates gives to total inverse scattering time

$$\tau_c^{-1} = \Gamma_{\text{e-lat}} + \Gamma_{\text{e-e}}, \tag{2.32}$$

where we take the electron-lattice scattering rate $\Gamma_{\text{e-lat}} = 2.0 \times 10^{15}$ [19] to be energy independent.

2.3.3 Plasma current and heating

The interaction between excited electrons and light can be modeled by treating the electrons as a gas of classical charged particles, an approach known as the Drude model. The resulting currents tend to defocus the indicent light pulse.

Consider a particle with charge q and mass m in an oscillating electromagnetic field which collides with other particles after an average time of τ_c. Assuming the velocity of the particle is small with respect to the group velocity of the light pulse we can write

$$m\frac{d\mathbf{v}}{dt} = q\mathbf{E} - m\frac{\mathbf{v}}{\tau_c}, \tag{2.33}$$

which can be written in the frequency domain as

$$m(\frac{1}{\tau_c} - i\omega)\mathbf{v}(\omega) = q\mathbf{E}(\omega). \tag{2.34}$$

The general solution is

$$\mathbf{v}(t) = \mathbf{v}_0 e^{-t/\tau_c} + \frac{q}{m}\int d\omega \frac{\tau_c}{1-i\omega\tau_c}\mathbf{E}(\omega)e^{-i\omega t}, \tag{2.35}$$

where $\mathbf{v}_0$ is an arbitrary constant. The second term thus gives the average particle velocity. Individual particles will have some additional nonvanishing randomly distributed thermal velocity, which gives rise to diffusion. The diffusion can be neglected, since it takes place on larger timescales than the plasma generation. In principle both electrons and holes will contribute to the current. However, the effective mass of the valence band holes ($m_v \approx 7.5m_e$) is much larger than that of the conduction band electrons ($m_c \approx 0.3m_e$) [2]. The contribution of the holes can therefore be neglected. The current can then be written as

$$\mathbf{J} = -e\rho\mathbf{v} = \frac{\rho e^2}{m}\int d\omega \frac{\tau_c}{1-i\omega\tau_c}\mathbf{E}(\omega)e^{-i\omega t}, \tag{2.36}$$

where ρ is the density of electrons in the conduction band. If we denote by a + superscript the positive frequency part we can write

$$i\left(\frac{\partial \mathbf{A}}{\partial \eta}\right)_{Plasma} = \frac{\mu_0}{k_0}\frac{\partial \mathbf{J}^+}{\partial \tau} = \frac{\mu_0 e}{k_0}\left(\frac{\partial \rho}{\partial \tau}\mathbf{v}_c^+ + \rho\frac{\partial \mathbf{v}_c^+}{\partial \tau}\right) \approx \frac{\mu_0 e\rho}{k_0}\frac{\partial \mathbf{v}_c^+}{\partial \tau}, \tag{2.37}$$

where we also make the reasonable assumption that the carrier density varies slowly with respect to the carrier wave frequency. We can express the change in velocity in terms of the envelope as

$$\begin{aligned}
\frac{\partial \mathbf{v}_c}{\partial t} =& \frac{e}{m_c}\int d\omega \frac{-i\omega\tau_c}{1-i\omega\tau_c}\tilde{\mathbf{E}}(\omega)e^{-i\omega t} \\
=& \frac{e}{2m_c}\int d\omega \frac{-i\omega\tau_c}{1-i\omega\tau_c}[\tilde{\mathbf{A}}(\omega-\omega_0)e^{ik_0 t} + \tilde{\bar{\mathbf{A}}}(\omega+\omega_0)e^{-ik_0 t}]e^{-i\omega t} \\
=& \frac{e}{2m_c}e^{i(k_0 z-\omega_0 t)}\int d\omega \frac{-i(\omega+\omega_0)\tau_c}{1-i(\omega+\omega_0)\tau_c}\tilde{\mathbf{A}}(\omega)e^{-i\omega t} \\
&+ \frac{e}{2m_c}e^{-i(k_0 z-\omega_0 t)}\int d\omega \frac{-i(\omega-\omega_0)\tau_c}{1-i(\omega-\omega_0)\tau_c}\tilde{\bar{\mathbf{A}}}(\omega)e^{-i\omega t}.
\end{aligned} \tag{2.38}$$

The same assumption for the envelope allows us to make the approximation

$$\frac{-i(\omega+\omega_0)\tau_c}{1-i(\omega+\omega_0)\tau_c}\tilde{\mathbf{A}}(\omega) \approx \frac{-i\omega_0\tau_c}{1-i\omega_0\tau_c}\tilde{\mathbf{A}}(\omega), \tag{2.39}$$

since $\mathbf{A}(\omega)$ is peaked around zero with a width smaller than ω_0. This amounts to taking only the carrier wave oscillations into account for the current. We can then go back into the time domain to get

$$\int d\omega \frac{-i(\omega+\omega_0)\tau_c}{1-i(\omega+\omega_0)\tau_c}\tilde{\mathbf{A}}(\omega)e^{-i\omega t} \approx \frac{-i\omega_0\tau_c}{1-i\omega_0\tau_c}\mathbf{A}(t). \tag{2.40}$$

Our final result is

$$\begin{aligned}
i\left(\frac{\partial \mathbf{A}}{\partial \eta}\right)_{Plasma} =& -\frac{\mu_0 e^2\rho}{2m_c k_0}\frac{i\omega_0\tau_c}{1-i\omega_0\tau_c}\mathbf{A} \\
=& -\frac{i\sigma\rho}{2}(1+i\omega_0\tau_c)\mathbf{A},
\end{aligned} \tag{2.41}$$

where $\sigma = \frac{e^2\mu_0}{k_0 m_c}\frac{\omega_0\tau_c}{1+\omega_0^2\tau_c^2}$ is known as the Drude conductivity. This expression also allows us to estimate the single photon absorption rate. The local photon density is $u = \frac{n_0^2\epsilon_0}{2\hbar\omega_0}|\mathbf{A}|^2$. The change along the η direction due to the plasma is

$$\frac{\partial u}{\partial \eta} = \frac{n_0^2\epsilon_0}{2\hbar\omega_0}\left(\frac{\partial \bar{\mathbf{A}}}{\partial \eta}\mathbf{A} + \bar{\mathbf{A}}\frac{\partial \mathbf{A}}{\partial \eta}\right) = -\frac{n_0^2\epsilon_0}{2\hbar\omega_0}\sigma\rho|\mathbf{A}|^2 = -\sigma\rho u. \tag{2.42}$$

By multiplying with the phase velocity of light c/n_0 we can get the rate at which photons are absorbed

$$\frac{\partial u}{\partial t} = -\sigma\rho\frac{cu}{n_0}. \tag{2.43}$$

This has to be divided by the total plasma density to get the rate at which a single electron absorbs a single photon. The final expression for the single photon absorption is then

$$W_{1\mathrm{p}} = \sigma\frac{cu}{n_0} = \frac{cn_0\epsilon_0\sigma}{2\hbar\omega_0}|\mathbf{A}|^2. \tag{2.44}$$

2.3.4 Refractive index

The change in refractive index due to the plasma defocusing can be found by going back to the wave equation

$$\nabla^2\tilde{\mathbf{E}} + \frac{\omega^2}{c^2}\left(1+\chi^{(1)}(\omega)\right)\tilde{\mathbf{E}} = -i\omega\mu_0\tilde{\mathbf{J}}. \tag{2.45}$$

If we take $\omega \approx \omega_0$ and approximate $\tilde{\mathbf{J}}(\omega_0) \approx \frac{e^2}{m}\frac{\tau_c}{1-i\omega_0\tau_c}\tilde{\rho}(0)\tilde{\mathbf{E}}(\omega_0)$ we can write it in the form

$$\nabla^2\tilde{\mathbf{E}} + \frac{\omega_0^2}{c^2}\left(1+\chi^{(1)}(\omega_0) - \frac{\rho e^2}{m\epsilon_0}\frac{\tau_c}{\omega_0^2\tau_c + i\omega_0}\right)\tilde{\mathbf{E}} = 0 \tag{2.46}$$

and we can see that the complex index of refraction at frequency ω_0 is

$$\tilde{n} = n + i\kappa = \sqrt{n_0^2 - \frac{\rho e^2}{m\epsilon_0}\frac{\tau_c}{\omega_0^2\tau_c + i\omega_0}} = \sqrt{n_0^2 - \frac{\omega_p^2}{\omega_0^2}\frac{\omega_0\tau_c}{\omega_0\tau_c + i}}, \tag{2.47}$$

where $\omega_p = \sqrt{\frac{\rho e^2}{m\epsilon_0}}$ is the plasma frequency. In our case $\omega_0\tau_c = 1.78$, so when $\omega_p > \omega_0$ the refractive index will have a significant imaginary part. Note that we thus take the Drude model into account as a frequency independent change to the refractive index. This approach is known to be numerically unstable when applied in finite difference time domain simulations. Out approach is not susceptible to this instability.

3 Numerical Methods

3.1 Electric field evolution

The equation we need to solve is of the Schrödinger form,

$$i\frac{\partial A}{\partial t} = \hat{\mathcal{H}}(t)A, \tag{3.1}$$

where the value of A is known for some time t_0. The formal solution [14] to this is given by

$$\begin{aligned} A(t) = &\lim_{N\to\infty} \exp\Big(-i\hat{\mathcal{H}}(t_0 + (N-1)\Delta t)\Delta t\Big) \cdots \exp\Big(-i\hat{\mathcal{H}}(t_0)\Delta t\Big) A(t_0) \\ =&\mathcal{T}\Big\{ \exp\Big(-i\int_{t_0}^{t} d\tau \hat{\mathcal{H}}(\tau)\Big)\Big\} A(t_0) \end{aligned} \tag{3.2}$$

where $\mathcal{T}$ denotes the time ordering operator and $\Delta t = (t - t_0)/N$. Now suppose that we take t to be close to t_0, then we can expand as follows

$$\begin{aligned} \mathcal{T}\Big\{ \exp\Big(-i\int_{t_0}^{t} d\tau \hat{\mathcal{H}}(\tau)\Big)\Big\} &= \mathcal{T}\Big\{ \exp\Big(-i\int_{t_0}^{t} d\tau \hat{\mathcal{H}}(t_0) + \frac{\partial \hat{\mathcal{H}}}{\partial t}(t_0)\tau + \cdots\Big)\Big\} \\ &= \exp\Big(-i\hat{\mathcal{H}}(t_0)(t-t_0) - i\frac{(t-t_0)^2}{2}\frac{\partial \hat{\mathcal{H}}}{\partial t}(t_0) + \mathcal{O}((t-t_0)^3)\Big) \\ &= \exp\Big(-i\hat{\mathcal{H}}(0)(t-t_0)\Big)(1 + \mathcal{O}((t-t_0)^2)), \end{aligned}$$

so by taking small time steps δt we can approximate the time evolution up to linear order in δt,

$$A(t_0 + \delta t) \approx \exp\Big(-i\hat{\mathcal{H}}(t_0)\delta t\Big) A(t). \tag{3.3}$$

Computing the exponential of an operator is generally very difficult. Suppose we can write the operator $\hat{\mathcal{H}}(t_0) = \hat{\mathcal{H}}_1 + \hat{\mathcal{H}}_2$, where $\hat{\mathcal{H}}_1$ and $\hat{\mathcal{H}}_2$ can be easily exponentiated:. Inserting this into the Baker–Campbell–Haussdorf formula yields

$$\exp\Big(-i\hat{\mathcal{H}}_1\delta t\Big) \exp\Big(-i\hat{\mathcal{H}}_2\delta t\Big) = \exp\Big(-i\hat{\mathcal{H}}(0)\delta t + \frac{\delta t^2}{2}[\hat{\mathcal{H}}_1, \hat{\mathcal{H}}_2] + \mathcal{O}(\delta t^3)\Big). \tag{3.4}$$

Thus, splitting $\hat{\mathcal{H}}(t_0)$ into easily exponentiable parts and taking small timesteps greatly speeds up computation at the price of a small error. An accuracy parameter δ will be used to determine how small the timesteps should be. In applying this to our simulations, we will split our operator into the following parts

$$\mathcal{H}_{\text{Diffraction}}(\mathbf{x}, \tau, \eta) = -\frac{\nabla_\perp^2}{2k_0}, \tag{3.5}$$

$$\mathcal{H}_{\text{Nonlinear}}(\mathbf{x}, \tau, \eta) = -k_0 n_2 \frac{\epsilon_0 c}{2}\Big[(1 - f_R)|\mathbf{A}|^2 + f_R \int_0^\infty dt' \mathcal{R}(t')|\mathbf{A}(t - t')|^2\Big], \tag{3.6}$$

$$\mathcal{H}_{\text{Drude}}(\mathbf{x}, \tau, \eta) = -\frac{i\sigma\rho(\mathbf{x}, \tau, \eta)}{2}(1 + i\omega_0\tau_c). \tag{3.7}$$

The last two of these are diagonal and thus easily exponentiable. For these two, the condition of "small timesteps" will be that the relative phase difference between two points is smaller than δ. The next section details a method to compute the exponential of the first operator.

3.1.1 Finite difference operator splitting

The exponential of a differential operator can be approximated by matrix splitting. This has been applied to the problem of femtosecond laser pulses in 3D [21]. The following is a formulation of the method for a general second order operator, which can then be applied to our problem.

Consider a general differential operator $\hat{Q}$ of an order no higher than two, acting on a function $A(x)$,

$$\hat{Q}(x)A(x) = \left[f_0(x) + f_1(x)\frac{\partial}{\partial x} + f_2(x)\frac{\partial^2}{\partial x^2}\right]A(x). \tag{3.8}$$

When doing computations this has to be converted to a discrete form. We can represent the interval by N gridpoints distributed evenly with a spacing Δx, such that $x_k = k\Delta x$, with $k = 0, 1, ..., N-1$. All functions are assumed to vanish outside of the interval. The operator $\hat{Q}$ can then be approximated using finite differences as follows

$$\begin{aligned}(\hat{Q}A)_k =& f_0(k\Delta x)A_k + f_1(k\Delta x)\frac{A_{k+1} - A_{k-1}}{2\Delta x} + f_2(k\Delta x)\frac{A_{k+1} - 2A_k + A_{k-1}}{(\Delta x)^2} \\ =& A_{k+1}\left[\frac{f_1(k\Delta x)}{2\Delta x} + \frac{f_2(k\Delta x)}{(\Delta x)^2}\right] + A_k\left[f_0(k\Delta x) - \frac{2f_2(k\Delta x)}{(\Delta x)^2}\right] + A_{k-1}\left[-\frac{f_1(k\Delta x)}{2\Delta x} + \frac{f_2(k\Delta x)}{(\Delta x)^2}\right] \\ =& c_k A_{k+1} + b_k A_k + a_k A_{k-1},\end{aligned} \tag{3.9}$$

where derivatives are approximated by difference quotients. We can thus write $\hat{Q}$ as a matrix acting on A written as a vector. We find

$$Q = \begin{pmatrix} b_0 & c_0 & 0 & 0 & 0 & 0 & \dots & 0 \\ a_1 & b_1 & c_1 & 0 & 0 & 0 & \dots & 0 \\ 0 & a_2 & b_2 & c_2 & 0 & 0 & \dots & 0 \\ 0 & 0 & a_3 & b_3 & c_3 & 0 & \dots & 0 \\ 0 & 0 & 0 & a_4 & b_4 & c_4 & \dots & 0 \\ 0 & 0 & 0 & 0 & a_5 & b_5 & \dots & 0 \\ \vdots & \vdots & \vdots & \vdots & \vdots & \vdots & \ddots & \vdots \\ 0 & 0 & 0 & 0 & 0 & 0 & \dots & b_{N-1} \end{pmatrix}, \qquad A = \begin{pmatrix} A_0 \\ A_1 \\ A_2 \\ A_3 \\ A_4 \\ A_5 \\ \vdots \\ A_{N-1} \end{pmatrix} \tag{3.10}$$

Now suppose we want to solve the following problem

$$i\frac{\partial A}{\partial t} = QA. \tag{3.11}$$

The formal solution is

$$A(t) = e^{-iQt}A(0), \tag{3.12}$$

so we need to find some way to compute the exponential for Q. We can split Q into two easily diagonalizable parts,

$$Q_{\text{even}} = \begin{pmatrix} b_0/2 & c_0 & 0 & 0 & 0 & 0 & \dots & 0 \\ a_1 & b_1/2 & 0 & 0 & 0 & 0 & \dots & 0 \\ 0 & 0 & b_2/2 & c_2 & 0 & 0 & \dots & 0 \\ 0 & 0 & a_3 & b_3/2 & 0 & 0 & \dots & 0 \\ 0 & 0 & 0 & 0 & b_4/2 & c_4 & \dots & 0 \\ 0 & 0 & 0 & 0 & a_5 & b_5/2 & \dots & 0 \\ \vdots & \vdots & \vdots & \vdots & \vdots & \vdots & \ddots & \vdots \\ 0 & 0 & 0 & 0 & 0 & 0 & \dots & b_{N-1}/2 \end{pmatrix} \tag{3.13}$$

$$Q_{\text{odd}} = \begin{pmatrix} b_0/2 & 0 & 0 & 0 & 0 & 0 & \dots & 0 \\ 0 & b_1/2 & c_1 & 0 & 0 & 0 & \dots & 0 \\ 0 & a_2 & b_2/2 & 0 & 0 & 0 & \dots & 0 \\ 0 & 0 & 0 & b_3/2 & c_3 & 0 & \dots & 0 \\ 0 & 0 & 0 & a_4 & b_4/2 & 0 & \dots & 0 \\ 0 & 0 & 0 & 0 & 0 & b_5/2 & \dots & 0 \\ \vdots & \vdots & \vdots & \vdots & \vdots & \vdots & \ddots & \vdots \\ 0 & 0 & 0 & 0 & 0 & 0 & \dots & b_{N-1}/2 \end{pmatrix} \tag{3.14}$$

From the Baker–Campbell–Haussdorf formula it follows that

$$\left(e^{-iQ_{\text{even}}t/N}e^{-iQ_{\text{odd}}t/N}\right)^N = e^{-i(Q_{\text{even}}+Q_{\text{odd}})t-\frac{t^2}{2N}[(Q_{\text{even}},Q_{\text{odd}}]+\mathcal{O}(N^{-2})}, \tag{3.15}$$

so we can approximate the solution to eq. 3.11 by splitting the operators and taking small time steps, alternating between Q_{even} and Q_{odd}. All that is left is to exponentiate the quasi-diagonal matrices Q_{even} and Q_{odd}. To do this it suffices to exponentiate a general 2×2 matrix,

$$M = \begin{pmatrix} b_k/2 & c_k \\ a_{k+1} & b_{k+1}/2 \end{pmatrix} \tag{3.16}$$

which gives

$$e^{-itM} = e^{-iqt}\begin{pmatrix} \cos(st) + i\frac{r}{s}\sin(st) & i\frac{r^2-s^2}{a_{k+1}s}\sin(st) \\ -i\frac{a_{k+1}}{s}\sin(st) & \cos(st) - i\frac{r}{s}\sin(st) \end{pmatrix} \tag{3.17}$$

where $q = (b_{k+1} + b_k)/4$, $r = (b_{k+1} - b_k)/4$ and $s = \sqrt{r^2 + c_k a_{k+1}}$. For this operator the conditions on time steps are $q\Delta t < \delta$ and $s\Delta t < \delta$.

3.1.2 Cylindrical Symmetry

In the case of cylindrical symmetry we can reduce the problem to 2+1 dimensions. We assume that the field is radially polarized, $\mathbf{A}(r, \theta, z, t) = A(r, z, t)\mathbf{e}_r$. We have $\Delta_\perp = \frac{\partial^2}{\partial r^2} + \frac{1}{r}\frac{\partial}{\partial r}$. In the notation of the previous section we thus have that $f_0(r) = 0$, $f_1(r) = \frac{1}{r}$ and $f_2(r) = 1$. We have to be careful with the divergence in f_1. Instead of the usual cylindrical coordinate chart with $r \in [0, \infty]$ and $\phi \in [0, 2\pi]$ one can take $r \in [-\infty, \infty]$ and $\phi \in [0, \pi]$ and impose that all functions are symmetric in $r = 0$. This gives $A_{-1} = A_1$, and thus the first derivative vanishes at the origin. Note that this also gives an additional coupling between A_0 and A_1, which can be absorbed into the even part.

3.1.3 Perfectly matched layer

The light scatters off the plasma to larger angles than those present in the incident beam. The implementation of diffraction implies that the electric field is set to zero outside the simulation space. The edges will thus act as as a perfect conductor, leading to unphysical reflections. Because the outgoing light is no longer relevant for the creation of plasma, it is desirable to eliminate the reflections by using an absorbing layer at the edge of the simulation space. This absorbing layer can be implemented by analytic continuation of the spatial coordinate at the edges of the domain, leading to exponential decay of propagating waves. This method is known as a perfectly matched layer (PML) [17]. To see how this

can be implemented in cylindrical coordinates one starts in 2D cartesian coordinates and transforms the derivatives as follows

$$\begin{aligned}\frac{\partial}{\partial x} &\to \frac{1}{S(r)}\frac{\partial}{\partial x},\\ \frac{\partial}{\partial y} &\to \frac{1}{S(r)}\frac{\partial}{\partial y},\end{aligned} \tag{3.18}$$

where $S(r) = 1 + i\sigma(r)$. Then the Laplacian transforms as

$$\begin{aligned}\frac{\partial^2}{\partial x^2} + \frac{\partial^2}{\partial y^2} = \nabla_\perp^2 \to &\frac{1}{S^2(r)}\nabla_\perp^2 - \frac{\partial S}{\partial r}\frac{1}{S^3(r)}\left(\frac{\partial r}{\partial x}\frac{\partial}{\partial x} + \frac{\partial r}{\partial y}\frac{\partial}{\partial y}\right)\\ =&\frac{1}{S^2(r)}\nabla_\perp^2 - \frac{\partial S}{\partial r}\frac{1}{S^3(r)}\frac{\partial}{\partial r}\\ =&\frac{1}{S^2(r)}\left[\frac{\partial^2}{\partial r^2} + \left(\frac{1}{r} - \frac{\partial S}{\partial r}\frac{1}{S(r)}\right)\frac{\partial}{\partial r}\right].\end{aligned} \tag{3.19}$$

A common choice for σ, which will be used in these simulations, is:

$$\sigma(r) = \begin{cases} 0 & \text{if } r \le r_{\text{PML}} \\ \sigma_{\max}\left(\frac{r - r_{\text{PML}}}{\Delta_{\text{PML}}}\right)^2 & \text{if } r > r_{\text{PML}} \end{cases}$$

such that the PML is in the region $[r_{\text{PML}}, r_{\max}]$ with width $\Delta_{\text{PML}} = r_{\max} - r_{\text{PML}}$.

3.2 Physical parameters

Parameter	Symbol	Value	Comment/reference
Silica band gap	Δ	9 eV	[8]
Electron-lattice collision rate	$\Gamma_{\text{e-lat}}$	2.0×10^{15} s^{-1}	[19]
Carrier recombination time	τ_r	150 fs	[1]
Conduction band effective mass	m_c	$0.3m_e$	[2]
Valence band mass	m_v	$7.5m_e$	[2]
Impact ionization coefficient	α	6.0×10^{15} s^{-1}	Chosen such that $\alpha > W_{1\text{p}}$ [13]
Nonlinear refractive index	n_2	$3.54 \times 10^{-20} m^2/W^2$	[16]
Fraction of Raman contribution	f_R	0.18	[6]
Raman oscillation time	ω_R^{-1}	12 fs	[23]
Raman damping time	Γ_R	50 fs	[23]

3.3 Input field

The incoming pulse is taken to be Gaussian in time and space.

$$A(r, \tau, \eta = 0) = A_0 \exp\left(-\frac{r^2}{w_i^2} - 2\log(2)\frac{t^2}{t_{\text{FWHM}}^2} - i\frac{k_0 r^2}{2R}\right), \tag{3.20}$$

where w_i is the initial beam waist, t_{FWHM} is the FWHM time of the laser pulse and $R = d + z_R^2/d$ is the curvature, with d the distance to the focus and $z_R = k_0 w_0^2/2$ the Rayleigh length for a beam waist w_0. Note that in experiments pulses are used that are Gaussian in air, not silica, so after the air to silica interface the pulse will no longer follow the path of a Gaussian beam. The distortions that result are known as spherical abberations. These are currently not taken into account in the simulations. The possible effects that spherical abberations might have will be discussed.

4 Results

To estimate the accuracy of the model we compare simulation results with transmission images of pump-probe experiments performed in UC Davis [20]. These experiments were carried out by sending a Gaussian pulse at a wavelength of 800 nm through a microscope objective with NA = 0.25 placed after a slit with a width of 250 μm. The writing depth was 500 μm. The pulses had a duration (FWHM) of 200 fs. To image the plasma a 400 nm probe pulse was sent through the sample from the side at different time delays. The width in the direction perpendicular to the slit was estimated to be 2 μm.

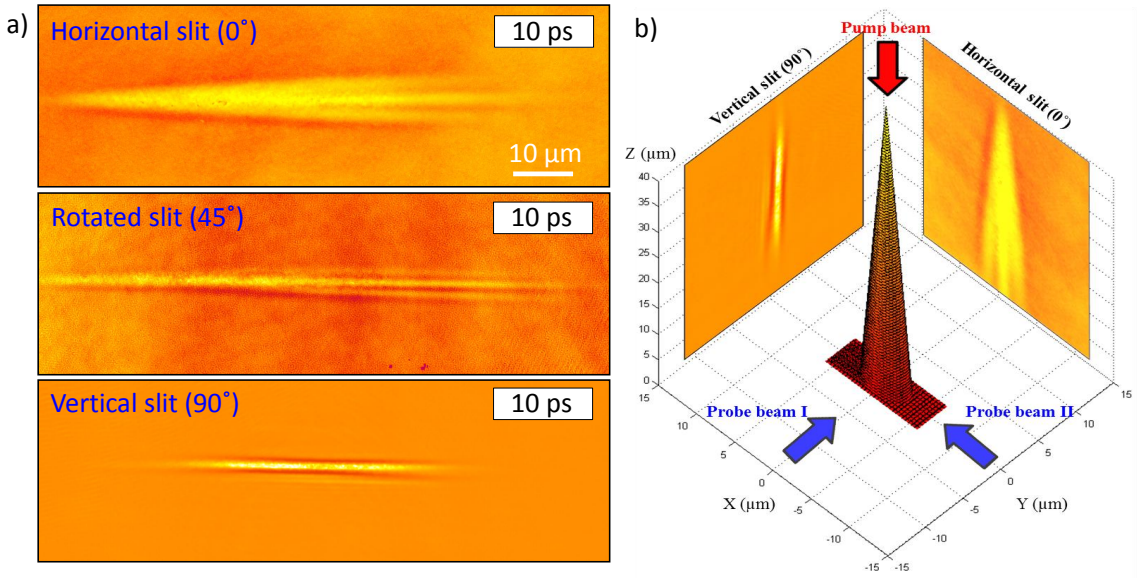

Figure 4.1: Transmission images for different orientations of the slit.

The transmission images for energies 2, 4 and 6 μJ and time delay 500 fs will be compared with simulations. Simulations were run at the three pulse energies with a duration of $t_{\text{FWHM}} = 200$ fs. The accuracy parameter was set to $\delta = 0.05$. To compare the results to the experiments, we take the plasma to have the final distribution from the simulations in the plane perpendicular to the probe pulse, and to be a uniform slab with a width of $2\mu m$ along the axis of the probe pulse. The transmission is then given by $T(r, z, t) = \exp(-4\pi\kappa(r, z, t)W/\lambda_0)$, where $W = 2\mu m$ is the width of the plasma slab, κ is the imaginary part of the refractive index for the probe light with a vacuum wavelength of $\lambda_0 = 400$ nm. For these images the electron-electron scattering contribution to the scattering rate is neglected. In this comparison diffraction effects are neglected, which is a good approximation since the real and imaginary modifications to the dielectric function are of the same size. This means that for plasma frequencies below the laser frequency little scattering occurs. The transmission images have the same scale as the simulation images. In all images the propagation direction of the pump pulse is from right to left.

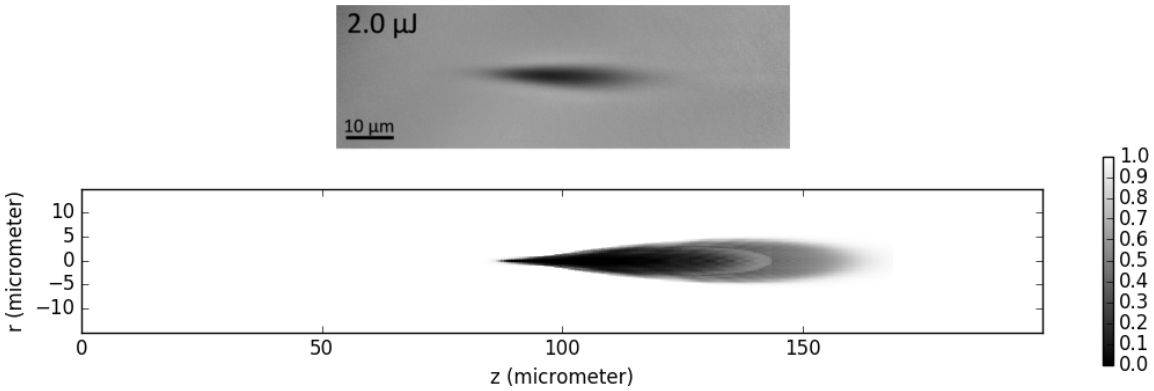

Figure 4.2: 2 μJ

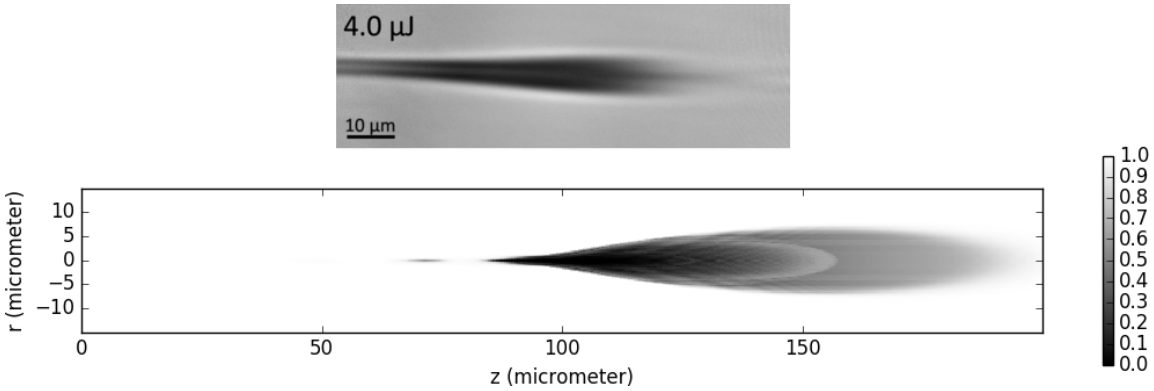

Figure 4.3: 4 μJ

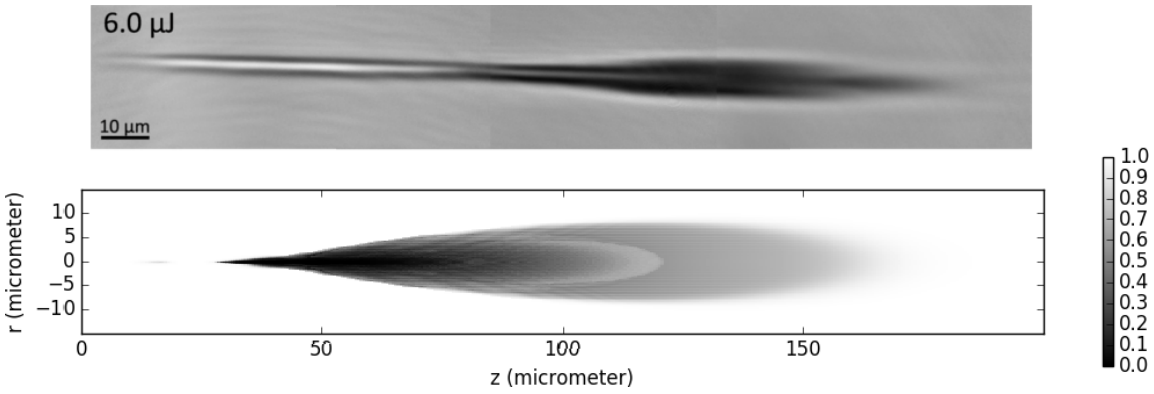

Figure 4.4: 6 μJ

The simulation profiles all have the same basic feather-like shape. The front of the pulse generates a small amount of electrons through SFI but not enough to scatter the light. The propagation of this part of the pulse is therefore unaffected by the plasma, and consequently only weakly dependent on the pulse energy. Increasing the power increases the distance from the focus at which plasma formation starts. The simulations consistently predict a larger plasma cloud than found experimentally. However, because the transmission profile is very sensitive to our assumptions about the thickness of the cloud along the probe axis it is difficult to draw conclusions from this. Another difference is the formation of a long tail at higher powers in experiments.

5 Conclusion & Discussion

In summary, a model was developed to simulate the interaction between femtosecond laser pulses and bulk silica. Starting from Maxwell's equations, the propagation of the electric field was computed by using the slowly varying envelope approximation in the co-moving frame to rewrite the wave equation into the Schroödinger equation. This equation was then supplemented with the Kerr effect and Raman scattering. Operator splitting methods were used to compute the evolution of the field. The electron plasma was described as a classical gas categorized into discrete energy levels. The Drude model was used to describe the interaction between the plasma and the electric field, taking into account the effect of the energy distribution of the electron gas on the scattering rate. The generation of plasma was computed using Keldysh's expression for the strong field ionization rate (SFI) and Rethfeld's multiple rate equation (MRE) for impact ionization. The simulations showed the interaction between Gaussian laser pulses and fused silica at different pulse energies.

The simulations presented assume that the pulse is Gaussian inside fused silica. In the experiment, spherical abberations due to the air-silica interface lead to a non-Gaussian pulse. Sun et al [18] found that such spherical abberation were responsible for the formation of long plasma channels. Spherical abberations stretch the focal volume and widen the beam waist, leading to a longer and thinner plasma. This may explain the differences between our simulation results and experimental observations. More detailed comparison between simulation and experiment thus requires that spherical aberration be taken into account. This can be done by simulating the propagation of a Gaussian pulse starting at the air to glass interface, and dynamically scaling the radial size of the simulation space to maximize resolution. The implementation of this dynamical scaling is explained in Appendix A. Further optimization (e.g. parallelization) might make it possible to adapt the code for (3+1)D simulations. Most of the computation time is spent on the MRE, so simulating the transmission of the probe pulse in (3+1)D could be done within reasonable times even without optimization.

The MRE assumes that the electrons can only occupy states which have an energy that is an integer multiple of the photon energy. The weakness of this assumption can be seen when the field-dependent critical energy starts dropping after the peak of the pulse has passed. When the critical energy passes the position of an energy bin, the electrons in that bin suddenly all ionize by scattering. This leads to a spike in impact ionization. In reality, electron-electron and electron-phonon scattering will smooth out the electron energy spectrum. A possible solution to this computational artifact would be to assume that electrons in energy bin j are uniformly distributed in the interval $[j\hbar\omega_0, (j+1)\hbar\omega_0)$ and adjusting the impact ionization rate accordingly. For example, suppose that the critical ionization energy is at $E_{\text{imp}}(j+\epsilon)\hbar\omega_0$, where $0 \leq \epsilon \leq 1$. Then the rate equation for the level j will be $\dot{\rho_j} = -(W_{1\text{p}} + (1-\epsilon)\alpha)\rho_j + W_{1\text{p}}\rho_{j-1}$.

The transmission profiles compared to experiment considered only the final distribution. In experiment, one can look at different time delays to examine how the plasma grows in time. To compare these to simulations one must consider the finite duration of the probe pulse, since different parts of the pulse will probe different plasma distributions. This could be done by a temporal convolution between the (normalized) intensity distribution and the transmission.

6 Acknowledgements

I'd like to thank Dries van Oosten and Javier Hernández-Rueda for supervising me, and always being available for questions I had. Secondly, I'd like to thank Denise Krol for the experimental data, which came from her lab, and for solving some problems I had with units in the literature. Thanks also to Jasper Smits for discussions on numerics over ping-pong and to everyone who listened to me ramble about operators.

Appendix A Dynamical radial scaling

To account for spherical abberations, the simulation should start at the air to silica interface. The beam be much wider at the interface than at the focus, where plasma generation takes place. To make sure that computation time and resolution are not wasted we can rescale the radial coordinate dynamically

$$\tilde{r} = \frac{r}{w(\eta)}, \quad \tilde{\eta} = \eta. \tag{A.1}$$

The derivatives then transform as

$$\frac{\partial}{\partial r} = \frac{\partial \tilde{r}}{\partial r}\frac{\partial}{\partial \tilde{r}} + \frac{\partial \tilde{\eta}}{\partial r}\frac{\partial}{\partial \tilde{\eta}} = \frac{1}{w(\tilde{\eta})}\frac{\partial}{\partial \tilde{r}} \tag{A.2}$$

$$\frac{\partial}{\partial \eta} = \frac{\partial \tilde{r}}{\partial \eta}\frac{\partial}{\partial \tilde{r}} + \frac{\partial \tilde{\eta}}{\partial \eta}\frac{\partial}{\partial \tilde{\eta}} = -\frac{r}{w^2(\eta)}\frac{\partial w}{\partial \eta}\frac{\partial}{\partial \tilde{r}} + \frac{\partial}{\partial \tilde{\eta}} = -\frac{\tilde{r}}{w(\eta)}\frac{\partial w}{\partial \eta}\frac{\partial}{\partial \tilde{r}} + \frac{\partial}{\partial \tilde{\eta}}. \tag{A.3}$$

So as one would expect from a coordinate transformation we get a fictitious force term, which is added to the right-hand side of the envelope equation as

$$i\left(\frac{\partial \mathbf{A}}{\partial \tilde{\eta}}\right)_{\text{ff}} = \frac{i\tilde{r}}{w(\eta)}\frac{\partial w}{\partial \eta}\frac{\partial \mathbf{A}}{\partial \tilde{r}}, \tag{A.4}$$

and the laplacian changes slightly

$$\nabla_\perp^2 = \frac{\partial}{\partial r^2} + \frac{1}{r}\frac{\partial}{\partial r} = \frac{1}{w^2(\tilde{\eta})}\left[\frac{\partial}{\partial \tilde{r}^2} + \frac{1}{\tilde{r}}\frac{\partial}{\partial \tilde{r}}\right]. \tag{A.5}$$

Putting them together we get

$$i\left(\frac{\partial \mathbf{A}}{\partial \tilde{\eta}}\right)_{\text{Diff+ff}} = \frac{1}{w^2(\tilde{\eta})}\left[\left(i\tilde{r}w(\eta)\frac{\partial w}{\partial \eta} - \frac{1}{2k_0\tilde{r}}\right)\frac{\partial}{\partial \tilde{r}} - \frac{1}{2k_0}\frac{\partial^2}{\partial \tilde{r}^2}\right]\mathbf{A}. \tag{A.6}$$

A convenient choice for $w(\eta)$ is the beam width of a Gaussian beam, $w(\eta) = w_0\sqrt{1 + \frac{\eta^2}{z_R^2}}$, where w_0 is the beam waist and z_R is the Rayleigh length.

References

[1] P. Audebert, Ph. Daguzan, A. Dos Santos, J. C. Gauthier, J. P. Geindre, S. Guizard, G. Hamoniaux, K. Krastev, P. Martin, G. Petite, and A. Antonetti. Space-time observation of an electron gas in sio_2. *Phys. Rev. Lett.*, 73:1990–1993, Oct 1994.

[2] James R. Chelikowsky and M. Schlüter. Electron states in α-quartz: A self-consistent pseudopotential calculation. *Phys. Rev. B*, 15:4020–4029, Apr 1977.

[3] B. H. Christensen and P. Balling. Modeling ultrashort-pulse laser ablation of dielectric materials. *Phys. Rev. B*, 79:155424, Apr 2009.

[4] Jasper Clarijs. Femtosecond laser nano-ablation of glass surfaces and their self-scattering effects. Master's thesis, 2016.

[5] A. Couairon and A. Mysyrowicz. Femtosecond filamentation in transparent media. *Physics Reports*, 441(24):47 – 189, 2007.

[6] A. Couairon, L. Sudrie, M. Franco, B. Prade, and A. Mysyrowicz. Filamentation and damage in fused silica induced by tightly focused femtosecond laser pulses. *Phys. Rev. B*, 71:125435, Mar 2005.

[7] E. N. Glezer and E. Mazur. Ultrafast-laser driven micro-explosions in transparent materials. *Applied Physics Letters*, 71(7):882–884, 1997.

[8] Javier Hernandez-Rueda, Jasper Clarijs, Dries van Oosten, and Denise M. Krol. The influence of femtosecond laser wavelength on waveguide fabrication inside fused silica. *Applied Physics Letters*, 110(16):161109, 2017.

[9] A. Kaiser, B. Rethfeld, M. Vicanek, and G. Simon. Microscopic processes in dielectrics under irradiation by subpicosecond laser pulses. *Phys. Rev. B*, 61:11437–11450, May 2000.

[10] L.V. Keldysh. Ionization in the field of a strong electromagnetic wave. *Zh. Eksp. Teor. Fiz.*, 20, May 1965.

[11] Rei Kitamura, Laurent Pilon, and Miroslaw Jonasz. Optical constants of silica glass from extreme ultraviolet to far infrared at near room temperature. *Appl. Opt.*, 46(33):8118–8133, Nov 2007.

[12] I. H. Malitson. Interspecimen comparison of the refractive index of fused silica∗,. *J. Opt. Soc. Am.*, 55(10):1205–1209, Oct 1965.

[13] B. Rethfeld. Unified model for the free-electron avalanche in laser-irradiated dielectrics. *Phys. Rev. Lett.*, 92:187401, May 2004.

[14] J.J. Sakurai. *Advanced Quantum Mechanics*. A-W series in advanced physics. Pearson Education, Incorporated, 1967.

[15] B C Stuart, M D Feit, S Herman, AM Rubenchik, BW Shore, and MD Perry. Nanosecond-to-femtosecond laser-induced breakdown in dielectrics. *Physical review B*, 53(4):1749, 1996.

[16] L. Sudrie, A. Couairon, M. Franco, B. Lamouroux, B. Prade, S. Tzortzakis, and A. Mysyrowicz. Femtosecond laser-induced damage and filamentary propagation in fused silica. *Phys. Rev. Lett.*, 89:186601, Oct 2002.

[17] D.M. Sullivan. *Electromagnetic Simulation Using the FDTD Method*. Wiley, 2013.

[18] Quan Sun, Hongbing Jiang, Yi Liu, Yongheng Zhou, Hong Yang, and Qihuang Gong. Effect of spherical aberration on the propagation of a tightly focused femtosecond laser pulse inside fused silica. *Journal of Optics A: Pure and Applied Optics*, 7(11):655, 2005.

[19] Kristian Wædegaard, Martin Frislev, and Peter Balling. Femtosecond laser excitation of dielectric materials: experiments and modeling of optical properties and ablation depths. *Applied Physics A*, 110(3):601–605, 2013.

[20] Jon J Witcher, Javier Hernandez-Rueda, and Denise M Krol. Fs-laser processing of glass: Plasma dynamics and spectroscopy. *International Journal of Applied Glass Science*, 6(3):220–228, 2015.

[21] Eli Yablonovitch and N. Bloembergen. Avalanche ionization and the limiting diameter of filaments induced by light pulses in transparent media. *Phys. Rev. Lett.*, 29:907–910, Oct 1972.

[22] Hao Zhang, Denise M. Krol, Jaap I. Dijkhuis, and Dries van Oosten. Self-scattering effects in femtosecond laser nanoablation. *Opt. Lett.*, 38(23):5032–5035, Dec 2013.

[23] Alex A. Zozulya, Scott A. Diddams, and Tracy S. Clement. Investigations of nonlinear femtosecond pulse propagation with the inclusion of raman, shock, and third-order phase effects. *Phys. Rev. A*, 58:3303–3310, Oct 1998.